# SPARSE AND MULTI-OBJECT POSE+SHAPE MODELING OF THE THREE-DIMENSIONAL SCOLIOTIC SPINE

*Robert Korez*[⋆†] *Benjamin Aubert*[‡] *Thierry Cresson*[‡] *Stefan Parent*[§]
*Tomaž Vrtovec*[†] *Jacques de Guise*[‡] *Samuel Kadoury*[⋆§]

[⋆] MedICAL, École Polytechnique de Montréal, Montréal, QC, Canada
[†] LIT, University of Ljubljana, Faculty of Electrical Engineering, Ljubljana, Slovenia
[‡] LIO, École de technologie supérieure, Centre de recherche du CHUM, Montréal, QC, Canada
[§] Centre de recherche du CHU Sainte-Justine, Montréal, QC, Canada

## ABSTRACT

Adolescent idiopathic scoliosis (AIS) is a complex three-dimensional (3-D) deformation of the trunk, which includes lateral deviation of the spine, asymmetric deformation and axial rotation of the vertebrae, deformation of the rib cage, and possibly of the pelvis. In order to analyze 3-D characteristics of spinal deformations related to AIS, we propose a coarse-to-fine 3-D modeling framework of the scoliotic spine from biplanar X-ray images. First, the spine centerline represented by a cubic spline is used as a data descriptor for the underlying sparse modeling approach to obtain an initial 3-D reconstruction. We then optimize a multi-object pose+shape model that uses the statistical pose and geometric shape variability from a training set of scoliotic spines, onto a set of adjusted spinal landmarks to obtain the final 3-D reconstruction. The performance was evaluated on a database of 844 AIS patients, yielding an overall mean root-mean-square Euclidean distance $2.48 \pm 0.68$ mm for the final 3-D reconstruction of the scoliotic spine.

***Index Terms***— Adolescent idiopathic scoliosis, multi-object pose+shape modeling, sparse modeling, 3-D spine reconstruction

## 1. INTRODUCTION

Spinal deformity pathologies such as adolescent idiopathic scoliosis (AIS) are complex three-dimensional (3-D) local and global deformations of the trunk. Described as a lateral deviation of the spine, AIS is combined with asymmetric deformation and axial rotation of the vertebrae, deformation of the rib cage, and possibly of the pelvis. As suggested by its name, the cause of AIS remains unknown and can occur at any time during the child's growth. The imaging modality of choice for the 3-D clinical assessment of AIS is biplanar radiography since it allows the acquisition of data in the natural standing posture while exposing the patient to a relatively low dose of ionizing radiation.

In order to analyze 3-D characteristics of spinal deformations related to AIS, which can be useful for the evaluation of the immediate effect of the treatment with the Boston brace system, pre- and postoperative comparison of spine instrumentation surgery and progression of scoliosis, several 3-D reconstruction methods from biplanar radiography have been developed. The standard approach for spine reconstruction is to manually identify anatomical landmarks on biplanar X-ray images and match their 3-D positions, however, it is considered subjective and time-consuming. In order to reduce the number of landmarks involved, a semi-automatic method using a parametric model of the vertebrae was proposed by Pomero et al. [1]. Humbert et al. [2] combined the parametric model of the vertebrae with the parametric model of the whole spine to reduce the identification of landmarks in the first level of 3-D reconstruction. However, in the second reconstruction level, a considerable interaction by the user was required for a fine 3-D reconstruction of the spine. To take into account the dependencies between adjacent vertebrae in terms of location, orientation and shape, an articulated statistical model of the spine was used by Moura et al. [3], and inferred with a spline representing the spine centerline to obtain its 3-D reconstruction. Recently, Lecron et al. [4] upgraded the articulated model with the one-class support vector machine regularization in order to rely on similarities computed with a non-Gaussian kernel.

In this paper, we propose a coarse-to-fine modeling framework for the 3-D reconstruction of the scoliotic spine from biplanar X-ray images. First, the spine centerline, which is represented by the cubic spline in terms of its control points and local polynomial coefficients, is used as a data descriptor for the underlying sparse modeling approach to obtain the initial 3-D reconstruction. By finding a sparse representation of the input descriptor, non-Gaussian errors (e.g. noisy and erroneous extracted centerlines) can be accounted for. We then

This work was supported by the Slovenian Research Agency under grants P2-0232, J2-5473, J7-6781 and J2-7118, and by the Canada Research Chairs.

adapt a multi-object pose+shape model proposed by Bossa and Olmos [5], where pose and shape variations are separately extracted, and then correlated to present a joint pose+shape model. In contrast to articulated models, pose parameters were represented by similarity transformations, separately for each vertebral level. To obtain the final 3-D reconstruction of the scoliotic spine, the pose+shape model is fitted to spine landmarks that were initially reconstructed by sparse modeling and later adjusted using either manual or semi-automatic image-based methods.

## 2. MATERIALS AND METHODS

### 2.1. Training database

The training database consists of $N$ pairs of biplanar X-ray images of AIS patients. For each patient, a 3-D reconstruction of its spine (17 vertebrae in total) was generated from 3-D anatomical landmarks using a parametric model-based method [1], and validated by an expert. Six anatomical landmarks were identified on each vertebra from the first thoracic (T1) to the last lumbar (L5), i.e. two landmarks at the center of the superior and inferior vertebral endplate, and four landmarks at the tips of both pedicles. Furthermore, each 3-D reconstruction was normalized against the spine height, i.e. the distance between the T1 superior endplate landmark, denoted by $\boldsymbol{l}_{T1}$, and the L5 inferior endplate landmark, denoted by $\boldsymbol{l}_{L5}$. A common (default) coordinate system for each 3-D reconstruction in the training database was established by applying the Gram-Schmidt orthonormalization procedure on a set of vectors $\{\boldsymbol{l}_{T1} - \boldsymbol{l}_{L5}, \boldsymbol{e}_2, \boldsymbol{e}_2 \times (\boldsymbol{l}_{T1} - \boldsymbol{l}_{L5})\}$, where $\boldsymbol{e}_2 = [0, 1, 0]^T$. Finally, matrix $\boldsymbol{R} = [\boldsymbol{r}_1, \boldsymbol{r}_2, \ldots, \boldsymbol{r}_N] \in \mathbb{R}^{3M \times N}$ represented 3-D spine reconstructions stacked side-by-side, where each $\boldsymbol{r}_i \in \mathbb{R}^{3M \times 1}$, $i = 1, 2, \ldots, N$, corresponded to the concatenation of 3-D coordinates of all $M = 6 \cdot 17$ ground truth landmarks from the $i$-th spine.

### 2.2. Sparse modeling

The coarse-to-fine modeling framework proposed in this work first uses the reconstructed spine centerline from biplanar X-ray images to obtain the coefficients of the cubic spline. A piecewise polynomial continuous curve $\boldsymbol{p} : [\xi_1, \xi_{J+1}] \subset \mathbb{R} \rightarrow \mathbb{R}^3$ is a cubic spline if each segment $\boldsymbol{p}_j = \boldsymbol{p}|_{[\xi_j, \xi_{j+1}]}$, $j = 1, 2, \ldots, J$, $\xi_1 < \xi_2 < \ldots < \xi_{J+1}$, has a 3-D representation $\boldsymbol{p}_j(t) = (p_{1,j}(t), p_{2,j}(t), p_{3,j}(t))$, where

$$p_{i,j}(t) = \sum_{k=1}^{4} (t - \xi_j)^{4-k} c_{i,j,k} \tag{1}$$

is a third degree polynomial for $i = 1, 2, 3$. From the input biplanar X-ray images, the corresponding spine centerline can be obtained using Hessian filters as proposed in [6] and manually corrected by an expert. Furthermore, endpoints of the spine centerline are used for its normalization to the common coordinate system (Sec. 2.1), while the cubic spline interpolation is used to find the cubic spline in terms of its control points $\xi_j$ and local polynomial coefficients $c_{i,j,k}$. The control points and coefficients are concatenated into vector $\boldsymbol{d} = [\xi_1, \xi_2, \ldots, \xi_{J+1}, c_{1,1,1}, c_{1,1,2}, \ldots, c_{3,J,4}]^T \in \mathbb{R}^{O \times 1}$, $O = (J+1) + 12J$, and they have a role as a data descriptor.

Sparse modeling is a widely used technique in many computer vision and engineering disciplines, including image processing, machine learning and shape modeling [7, 8]. Its standard formulation is a non-convex optimization problem, which is in practice solved by heuristics like alternating minimization, gradient descent or their variants. The goal of sparse modeling is to compute a sparse representation of the given input data from an overcomplete dictionary, i.e. to represent an input vector approximately as a weighted linear combination of a small number of basis vectors that usually form an overcomplete set. Let the overcomplete dictionary be represented with matrix $\boldsymbol{D} = [\boldsymbol{d}_1, \boldsymbol{d}_2, \ldots, \boldsymbol{d}_N] \in \mathbb{R}^{O \times N}$, where $\boldsymbol{d}_i \in \mathbb{R}^{O \times 1}$ is a cubic spline descriptor that represents the ground truth spine centerline of the $i$-th spine in the training database, and let vector $\boldsymbol{d} \in \mathbb{R}^{O \times 1}$ represent the cubic spline descriptor of the input spine centerline. The problem of finding a sparse representation of the input descriptor $\boldsymbol{d}$ in the given overcomplete dictionary $\boldsymbol{D}$ can be formulated as

$$\begin{aligned} \{\boldsymbol{x}^*, \boldsymbol{e}^*\} = \underset{\{\boldsymbol{x}, \boldsymbol{e}\}}{\arg\min} \left(\lambda_1 \cdot \|\boldsymbol{x}\|_1 + \lambda_2 \cdot \|\boldsymbol{e}\|_1\right) \\ \text{subject to } \|\boldsymbol{d} - (\boldsymbol{D} \cdot \boldsymbol{x} + \boldsymbol{e})\|_2 \leq \varepsilon, \end{aligned} \tag{2}$$

where $\boldsymbol{x} \in \mathbb{R}^{N \times 1}$ represents weights for the training database and $\boldsymbol{e} \in \mathbb{R}^{O \times 1}$ represents errors in the input descriptor. Furthermore, $\lambda_1$ and $\lambda_2$ control how sparse $\boldsymbol{x}$ and $\boldsymbol{e}$ are, respectively, and $\varepsilon$ accounts for the possible small noise in the data [8]. Once the sparse representation $\boldsymbol{x}^*$ of the input descriptor $\boldsymbol{d}$ is computed via Eq. 2, the initial 3-D model of the scoliotic spine is obtained by $\boldsymbol{R} \cdot \boldsymbol{x}^*$.

### 2.3. Multi-object pose+shape refinement

In order to obtain a more accurate and personalized 3-D reconstruction of the scoliotic spine, the model is refined by optimizing a multi-object pose+shape model trained on the database of previously reconstructed spine shapes described in Sec. 2.1. The model is optimized by selecting the pose and shape variations observed in the training set in order to fit the model to a set of adjusted landmarks. These adjusted landmarks are obtained by first projecting the initially reconstructed landmarks onto biplanar X-ray images and then refined using anatomical features based on semi-automatic [9] or manual approaches.

To construct a multi-object pose+shape model of the spine, we adapt a method proposed by Bossa and Olmos [5], which was successfully applied to segment lumbar vertebrae [10]. Let vectors $\boldsymbol{m} = [\boldsymbol{m}_1^T, \boldsymbol{m}_2^T, \ldots, \boldsymbol{m}_{17}^T]^T \in \mathbb{R}^{3M \times 1}$ and $\boldsymbol{m}_j \in \mathbb{R}^{3 \cdot 14 \times 1}$, $j = 1, 2, \ldots, 17$, represent the mean

spine and the mean $j$-th vertebra, respectively, of the training database $\boldsymbol{R}$ (Sec. 2.1). The pose of each $j$-th vertebra $\boldsymbol{r}_{i,j} \in \mathbb{R}^{3\cdot 14\times 1}$ from $i$-th spine $\boldsymbol{r}_i$ is characterized by the similarity transformation $\mathcal{S}_{i,j}$ that best fits $\boldsymbol{m}_j$ into $\boldsymbol{r}_{i,j}$ by Procrustes superimposition. For each vertebra, the mean similarity transformation $\mathcal{M}_j$ (i.e. the Fréchet mean) and residuals $\boldsymbol{t}_{i,j} = \log(\mathcal{M}_j^{-1} \circ \mathcal{S}_{i,j}) \in \mathbb{R}^{7\times 1}$ in the tangent space of the similarity group are obtained. Therefore, the pose feature vector of $i$-th spine is represented by $\boldsymbol{t}_i = [\boldsymbol{t}_{i,1}^T, \boldsymbol{t}_{i,2}^T, \ldots, \boldsymbol{t}_{i,17}^T]^T \in \mathbb{R}^{U\times 1}$, $U = 7 \cdot 17$. In order to capture geometric shape variations, the shape feature vector of $i$-th spine is represented by $\boldsymbol{s}_i = [\boldsymbol{s}_{i,1}^T, \boldsymbol{s}_{i,2}^T, \ldots, \boldsymbol{s}_{i,17}^T]^T \in \mathbb{R}^{3M\times 1}$, where $\boldsymbol{s}_{i,j} = \mathcal{S}_{i,j}^{-1}(r_{i,j}) \in \mathbb{R}^{3\cdot 14\times 1}$. A multi-object pose+shape feature vector of $i$-th spine can be therefore represented by $\boldsymbol{f}_i = [\boldsymbol{t}_i^T, \boldsymbol{s}_i^T]^T \in \mathbb{R}^{V\times 1}$, $V = U + 3M$. After extracting the pose and shape features from all spines in the training database, the principal component analysis (PCA) is applied to $\boldsymbol{F} = [\boldsymbol{f}_1, \boldsymbol{f}_2, \ldots, \boldsymbol{f}_N]^T \in \mathbb{R}^{N\times V}$. The PCA decomposition results in principal coefficients $\boldsymbol{P} = [[\boldsymbol{p}_1^T, \boldsymbol{q}_1^T]^T, [\boldsymbol{p}_2^T, \boldsymbol{q}_2^T]^T, \ldots, [\boldsymbol{p}_C^T, \boldsymbol{q}_C^T]^T] \in \mathbb{R}^{V\times C}$ and corresponding variances $\boldsymbol{\lambda} = [\lambda_1, \lambda_2, \ldots, \lambda_C] \in \mathbb{R}^{C\times 1}$, $C = V - 1$, where $\boldsymbol{p}_i = [p_{1,i}, p_{2,i}, \ldots, p_{U,i}]^T \in \mathbb{R}^{U\times 1}$ and $\boldsymbol{q}_i = [q_{1,i}, q_{2,i}, \ldots, q_{3M,i}]^T \in \mathbb{R}^{3M\times 1}$. Furthermore, let vectors $\boldsymbol{p}_{i,j} = [p_{j_1,i}, p_{j_2,i}, \ldots, p_{j_7,i}]^T \in \mathbb{R}^{7\times 1}$ and $\boldsymbol{q}_{i,j} = [q_{j_1,i}, q_{j_2,i}, \ldots, q_{j_{3\cdot 14},i}]^T \in \mathbb{R}^{3\cdot 14\times 1}$ denote principal coefficients that correspond to the pose and shape parameters, respectively, of $j$-th vertebra. The multi-object pose+shape model is then defined as $\mathfrak{S}(\boldsymbol{\mu}) = [\mathfrak{s}_1(\boldsymbol{\mu})^T, \mathfrak{s}_2(\boldsymbol{\mu})^T, \ldots, \mathfrak{s}_{17}(\boldsymbol{\mu})^T]^T \in \mathbb{R}^{3M\times 1}$, where

$$\mathfrak{s}_j(\boldsymbol{\mu}) = \mathcal{T}_j\left(\boldsymbol{m}_j + [\boldsymbol{q}_{1,j}, \boldsymbol{q}_{2,j}, \ldots, \boldsymbol{q}_{\widetilde{C},j}] \cdot \boldsymbol{\mu}\right), \quad (3)$$

is the pose+shape model of $j$-th vertebra,

$$\mathcal{T}_j = \mathcal{M}_j \circ \exp\left([\boldsymbol{p}_{1,j}, \boldsymbol{p}_{2,j}, \ldots, \boldsymbol{p}_{\widetilde{C},j}] \cdot \boldsymbol{\mu}\right) \quad (4)$$

is the similarity transformation, and $\boldsymbol{\mu} = [\mu_1, \mu_2, \ldots, \mu_{\widetilde{C}}]^T \in \mathbb{R}^{\widetilde{C}\times 1}$, $\widetilde{C} \ll C$, is a vector of weights.

Let $\boldsymbol{w} = [\boldsymbol{u}^T, \boldsymbol{v}^T]^T \in \mathbb{R}^{3(P+R)\times 1}$ denote a vector, where $\boldsymbol{u} \in \mathbb{R}^{3P\times 1}$ represents the concatenation of 3-D coordinates of $P$ out of $M$ initially reconstructed landmarks that were adequately adjusted either manually by an expert or semi-automatically using image-based methods, and $\boldsymbol{v} \in \mathbb{R}^{3R\times 1}$ represents the concatenation of 3-D coordinates of $R$ sampled points along the spine centerline that was extracted from the initial reconstruction. The problem of aligning model $\mathfrak{S}(\boldsymbol{\mu})$ to landmarks in $\boldsymbol{w}$ can be formulated as

$$\boldsymbol{\mu}^* = \arg\min_{\boldsymbol{\mu}} \|\boldsymbol{w} - \mathcal{E}(\mathfrak{S}(\boldsymbol{\mu}))\|_2, \quad (5)$$

where $\mathcal{E}$ extracts a subset of landmarks in $\mathfrak{S}(\boldsymbol{\mu})$ that correspond to landmarks in $\boldsymbol{w}$. The final 3-D reconstruction of the scoliotic spine $\mathfrak{S}(\boldsymbol{\mu}^*)$ is obtained by minimizing Eq. 5 using the covariance matrix adaptation evolution strategy algorithm [11].

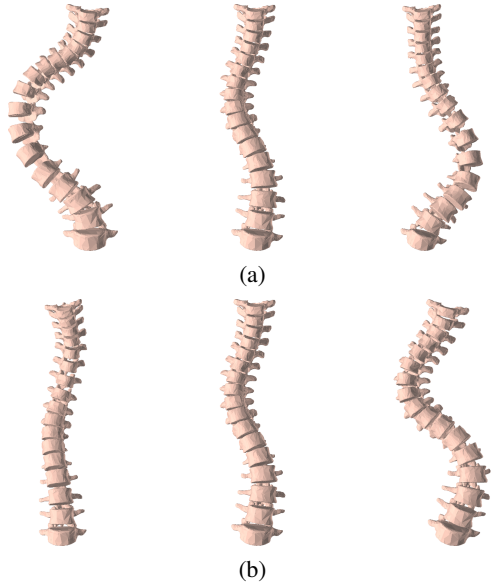

**Fig. 1**. Multi-object pose+shape variations described by changing the weights corresponding to the first two principal modes by (a) $-3\sqrt{\lambda_1}, 0, 3\sqrt{\lambda_1}$, and (b) $-3\sqrt{\lambda_2}, 0, 3\sqrt{\lambda_2}$.

## 3. RESULTS

The proposed method was evaluated on a group of $N = 844$ AIS patients using a leave-one-out evaluation scheme. An important aspect of the reconstruction process is its dependence to several parameters. Therefore, we analyzed the sensitivity of the algorithm against changes in parameters on a random subgroup of 211 out of 844 AIS patients, and optimal values were set to $J = 16$ (Sec. 2.2), $\lambda_1 = 1$, $\lambda_2 = 10$ and $\varepsilon = 0.0025$ (Eq. 2), and $\widetilde{C}$ (Eqs. 3 and 4) was set to account for $99.5\%$ of the observed variance in the data. Furthermore, depending on the severity of scoliosis, on average $P = 20$ initially reconstructed landmarks were either manually or automatically adjusted for the fine 3-D reconstruction of the scoliotic spine using the multi-object pose+shape model. To illustrate different deformation modes retrieved using the multi-object pose+shape model, three models were reconstructed for each of the first two principal modes (Fig. 1). Visual inspection revealed that the modes represent clinically relevant deformation paradigms, i.e. the first mode appears to be associated with changes in the major (thoracic or lumbar) curve, while the second mode with changes in the double (thoracolumbar) curve.

The 3-D reconstruction performance of the proposed framework was evaluated by the Euclidean distance (ED), computed between the reconstructed and corresponding ground truth landmarks (6 landmarks per vertebra, $6 \cdot 17 = 102$ landmarks in total). The overall reconstruction performance in terms of mean root-mean-square (RMS) $\pm$ standard deviation was ED $= 2.87 \pm 0.85$ mm and ED $= 2.48 \pm 0.68$ mm for the initial and final reconstruction,

**Table 1**. Summary of 3-D reconstruction results compared to Principal component analysis (PCA) modeling in terms of the Euclidean distance (ED) between landmarks for different spinal curve types according to the Lenke classification at different spine regions, reported as mean root-mean-square $\pm$ standard deviation.

| Lenke type | Spine region | Sparse modeling (mm) | Pose+shape modeling (mm) | PCA modeling (mm) |
|---|---|---|---|---|
| 1 | thoracic | $2.71 \pm 1.05$ | $2.21 \pm 0.74$ | $6.15 \pm 2.38$ |
| | lumbar | $3.10 \pm 1.12$ | $2.82 \pm 1.05$ | $7.24 \pm 3.20$ |
| 2 | thoracic | $2.90 \pm 0.93$ | $2.44 \pm 0.82$ | $6.29 \pm 2.27$ |
| | lumbar | $3.12 \pm 0.78$ | $2.81 \pm 0.81$ | $7.32 \pm 3.10$ |
| 3 | thoracic | $2.57 \pm 0.63$ | $2.09 \pm 0.48$ | $6.09 \pm 2.12$ |
| | lumbar | $3.01 \pm 0.69$ | $2.74 \pm 0.59$ | $6.95 \pm 2.63$ |
| 4 | thoracic | $2.86 \pm 0.75$ | $2.35 \pm 0.61$ | $6.36 \pm 2.54$ |
| | lumbar | $3.13 \pm 0.91$ | $2.94 \pm 0.86$ | $7.24 \pm 2.66$ |
| 5 | thoracic | $2.65 \pm 0.73$ | $2.16 \pm 0.48$ | $6.40 \pm 1.99$ |
| | lumbar | $3.33 \pm 0.97$ | $3.26 \pm 1.02$ | $7.70 \pm 2.94$ |
| 6 | thoracic | $2.64 \pm 0.85$ | $2.16 \pm 0.56$ | $6.82 \pm 2.84$ |
| | lumbar | $3.49 \pm 1.24$ | $3.38 \pm 1.16$ | $8.58 \pm 4.11$ |
| | **Overall** | $\mathbf{2.87 \pm 0.85}$ | $\mathbf{2.48 \pm 0.68}$ | $\mathbf{6.71 \pm 2.42}$ |

respectively, which represents a statistically significant reduction in error between both steps ($p < 0.01$). Detailed results of 3-D reconstructions for six different classes of AIS deformations according to the Lenke classification [12] are presented and compared to a PCA modeling approach in Table 1. Furthermore, in terms of errors for landmarks on vertebral endplates and pedicles, the final overall mean RMS was $1.51$ mm and $2.66$ mm, respectively. The performance of the proposed framework is therefore superior or comparable to the results reported by existing studies, as Moura et al. [3] reported a mean RMS of $1.20$ mm (vertebral endplates) and $3.40$ mm (pedicles) when evaluating reconstruction errors in 30 scoliotic spines, while Lecron et al. [4] reported $1.55$ mm (vertebral endplates) and $3.51$ mm (pedicles) for 100 scoliotic spines. According to the obtained results and comparison to existing methods, we can conclude that the results obtained by the proposed framework are highly accurate.

## 4. CONCLUSION

In this paper, we presented a framework to model the scoliotic spine in 3-D. First, the spine centerline is used as a data descriptor for the underlying sparse modeling approach to obtain the initial 3-D reconstruction. Afterwards, a multi-object pose+shape model is fitted to adjusted spine landmarks in order to obtain the final 3-D reconstruction of the scoliotic spine. The framework was validated on a large dataset of 844 patients with six different spinal curve types according to the Lenke classification of AIS.

Our future work will include dictionary learning technique to compute a compact codebook representing the original dictionary of ground truth cubic splines, and characterization of shapes (i.e. vertebrae) by configuration matrices that form the Procrustes shape space [5] for the sparse and multi-object modeling steps, respectively.

## 5. REFERENCES


[1] V. Pomero, D. Mitton, S. Laporte, J.A. de Guise, and W. Skalli, "Fast accurate stereoradiographic 3D-reconstruction of the spine using a combined geometric and statistic model," *Clin. Biomech.*, vol. 19, no. 3, pp. 240–247, 2004.

[2] L. Humbert, J.A. de Guise, B. Aubert, B. Godbout, and W. Skalli, "3D reconstruction of the spine from biplanar X-rays using parametric models based on transversal and longitudinal inferences," *Med. Eng. Phys.*, vol. 31, no. 6, pp. 671–687, 2009.

[3] D.C. Moura, J. Boisvert, J.G. Barbosa, H. Labelle, and J.M. Tavares, "Fast 3D reconstruction of the spine from biplanar radiographs using a deformable articulated model," *Med. Eng. Phys.*, vol. 33, no. 8, pp. 924–933, 2011.

[4] F. Lecron, J. Boisvert, S. Mahmoudi, H. Labelle, and M. Benjelloun, "Three-dimensional spine model reconstruction using one-class SVM regularization," *IEEE Trans. Biomed. Eng.*, vol. 60, no. 11, pp. 3256–3264, 2013.

[5] M.N. Bossa and S. Olmos, "Multi-object statistical pose+shape models," in *Proc. 4th IEEE International Symposium on Biomedical Imaging: From Nano to Macro*, 2007, pp. 1204–1207.

[6] S. Kadoury, F. Cheriet, and H. Labelle, "Segmentation of scoliotic spine silhouettes from enhanced biplanar X-rays using a prior knowledge Bayesian framework," in *Proc. 6th IEEE International Symposium on Biomedical Imaging: From Nano to Macro*, 2009, pp. 478–481.

[7] J. Wright, A.Y. Yang, A. Ganesh, S.S. Sastry, and Y. Ma, "Robust face recognition via sparse representation," *IEEE Trans. Pattern Anal. Mach. Intell.*, vol. 31, no. 2, pp. 210–227, 2009.

[8] G Wang, S. Zhang, H. Xie, D.N. Metaxas, and L. Gu, "A homotopy-based sparse representation for fast and accurate shape prior modeling in liver surgical planning," *Med. Image Anal.*, vol. 19, no. 1, pp. 176–186, 2015.

[9] S. Kadoury, F. Cheriet, and H. Labelle, "Personalized X-ray 3-D reconstruction of the scoliotic spine from hybrid statistical and image-based models," *IEEE Trans. Med. Imag.*, vol. 28, no. 9, pp. 1422–1435, 2009.

[10] A. Rasoulian, R. Rohling, and P. Abolmaesumi, "Lumbar spine segmentation using a statistical multi-vertebrae anatomical shape+pose model," *IEEE Trans. Med. Imag.*, vol. 32, no. 10, pp. 1890–1900, 2013.

[11] N Hansen and A. Ostermeier, "Completely derandomized self-adaptation in evolution strategies," *Evol. Comput.*, vol. 9, no. 2, pp. 159–195, 1999.

[12] L.G. Lenke, R.R. Betz, J. Harms, K.H. Bridwell, D.H. Clements, T.G. Lowe, and K. Blanke, "Adolescent idiopathic scoliosis: a new classification to determine extent of spinal arthrodesis," *J. Bone. Joint. Surg. Am.*, vol. 83-A, no. 8, pp. 1169–1181, 2001.